


 Cite this: *RSC Adv.*, 2024, 14, 39867

Thermogravimetric analysis of commercial tungsten molecular precursors for vapor phase deposition processes†

 Taylor M. Currie,^a Terrick McNealy-James,^{bc} S. Novia Berriel,^{bc} Konstantin Preradovic,^a Alfred P. Sattelberger,^a Parag Banerjee,^b and Titel Jurca^{abd}

Thin films and coatings based on Group 6 metal tungsten (W) have garnered intense interest for applications including catalysis, lubrication, and solar energy. Due to its selectivity and conformality, atomic layer deposition (ALD) has emerged as a key route towards oxides, dichalcogenides, and elemental metal films of W. A key component of the ALD process is the appropriate selection of molecular precursors. Thermogravimetric analysis (TGA) is the primary sorting criterion for precursor suitability and helps delineate probable ALD temperature windows, sublimation/vaporization kinetics, and parameters of decomposition. Currently, a majority of the W materials growth literature is traced to a grouping of commercially available volatile molecular precursors. However, no comprehensive thermochemical analysis exists for all of these precursors, hampering a meaningful direct comparison. Herein, we present an extensive thermogravimetric analysis and direct comparison of commercial volatile W molecular precursors. We report probable ALD temperature windows, enthalpies of sublimation (ΔH_{sub}), activation energies (E_a), and evaluate thermal stress. Our findings highlight several commercial precursors yet to be reported for ALD growth, but featuring thermochemical properties falling within our suitable observed parametric ranges indicative of potential/viable deposition processes.

 Received 10th October 2024
 Accepted 2nd December 2024

DOI: 10.1039/d4ra07284g

rsc.li/rsc-advances

1. Introduction

Due to broad ranging applications in electronics, sensing, solar energy materials, lubricants and catalysis, thin films based on the Group 6 metal tungsten (W) have garnered intense interest in recent years.^{1–7} The majority of the focus has been on the oxides WO_x ($2 \leq x \leq 3$) and dichalcogenides WE_2 ($\text{E} = \text{S}, \text{Se}, \text{Te}$), and to a lesser extent elemental metal, metal nitride, and metal carbide films. While chemical vapor deposition (CVD) has been the traditional preparative route, limitations in thickness control and conformality over larger domains has ushered in the development of atomic layer deposition (ALD)-based routes for these materials. Concomitantly, this has generated interest in the development of suitable W-based molecular precursors to

enable film growth. As ALD precursors are often highly reactive and air- and moisture-sensitive, requiring significant background in molecular inorganic synthesis, most end-users are heavily reliant on a limited group of commercial precursors.

ALD is a vapor-phase process that utilizes alternating pulses of volatilized chemical precursors containing the elemental components of interest in the growing film (typically a metal, and an oxidant or reductant).^{8,9} An example of the growth of

^aDepartment of Chemistry, University of Central Florida, Orlando, Florida 32816, USA. E-mail: titel.jurca@ucf.edu
^bRenewable Energy and Chemical Transformations Cluster, University of Central Florida, Orlando, Florida 32816, USA

^cDepartment of Materials Science and Engineering, University of Central Florida, Orlando, Florida 32816, USA

^dNanoScience & Technology Center, University of Central Florida, Orlando, Florida 32826, USA

^eFlorida Solar Energy Center, University of Central Florida, Cocoa, Florida 32922, USA

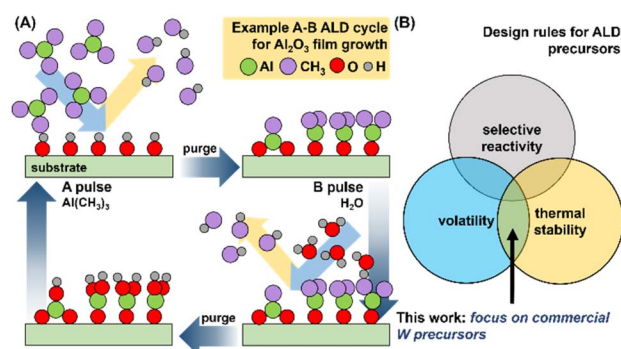
 † Electronic supplementary information (ESI) available. See DOI: <https://doi.org/10.1039/d4ra07284g>


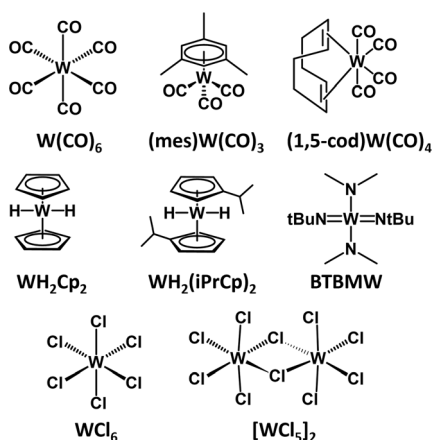
Fig. 1 (A) Schematic representation of growth sequence for Al_2O_3 film by ALD using $\text{Al}(\text{CH}_3)_3$ and H_2O in an A–B cycle; an “ideal” ALD process. (B) Venn diagram of desirable characteristics for viable ALD precursors.



Al_2O_3 with molecular precursors $\text{Al}(\text{CH}_3)_3$ and H_2O in an A-B cycle, one of the best understood ALD processes, is highlighted in Fig. 1A.

Optimal process parameters for ALD growth (temperature, pulse duration, number of cycles) are dependent on the physicochemical properties of both the precursors and the substrate. ALD precursor viability is predicated on three key attributes: (i) volatility, (ii) thermal stability, and (iii) selective surface reactivity (Fig. 1B).^{10,11} Testing all three attributes naturally requires the use of an ALD reactor, and multi-parametric optimization (*vide supra*) and often significant amounts of precursors (gram scale). However, volatility and thermal stability are the primary criteria before surface reactivity can even be evaluated. Thermogravimetric analysis (TGA) only requires milligram amounts of analyte and can rapidly confirm both volatility and thermal stability of molecular precursors. This can facilitate rapid down-selection of precursor without the need for immediate synthetic scale-up and valuable ALD reactor time. Comprehensive multi-parameter screening can also provide operational TGA “temperature windows”, and related sublimation parameters such as enthalpy of sublimation (ΔH_{sub}), activation energy (E_a), and 1 Torr temperatures; all valuable metrics which can facilitate comparisons between larger pools of precursors and inform operational parameters for ALD growth of thin films. With these values in hand, researchers can select the appropriate precursor(s) for their targeted ALD processes.

In this paper, we report the thermochemical properties of a group of commercial W precursors (Scheme 1) evaluated using TGA. The chosen molecules can be broadly categorized according to their general ligand classes; carbonyls [$\text{W}(\text{CO})_6$, (1,5-cod) $\text{W}(\text{CO})_4$], cyclopentadienyl [WH_2Cp_2 , $\text{WH}_2(\text{iPrCp})_2$], chlorides [$[\text{WCl}_5]_2$, WCl_6], and amino/imido [BTBMW]. While the reporting of thermochemical parameters for these precursors has been treated with varying degrees of rigor spanning multiple publications over several decades, a systematic and comparative investigation has been lacking. Compounded with the fact that TGA-obtained data is dependent on a multitude of experimental parameters, such as the amount of sample



Scheme 1 Commercially available W-based precursors subjected to non-isothermal TGA in this report.

analyzed, the temperature ramp rate, the instrument, pan material, and the specific environmental conditions, including atmosphere, means that there is no single cohesive source of ALD-relevant thermochemical data for users of these commercial precursors. We report herein a rigorous non-isothermal TGA study of eight commercial W molecular precursors (Scheme 1) for vapor phase processes highlighting measured TGA temperature windows (*we define this as the region between 5% and 95% of observed mass loss*), enthalpies of sublimation (ΔH_{sub}), activation energies (E_a), and 1 Torr temperatures. For simplicity and continuity, as most of the precursors are solids at room temperature, we report enthalpies of sublimation (ΔH_{sub}). However, precursors $\text{WH}_2(\text{iPrCp})_2$ and BTBMW are liquids and in these cases, it should be noted we are referring to enthalpies of vaporization (ΔH_{vap}).

For the remainder of the manuscript, we will use ΔH_{sub} as a comprehensive term relating to the enthalpies associated with the precursors entering the gas phase. Additionally, we recognize that commercially available WF_6 has been successfully used for ALD growth of W and WS_2 films.^{12,13} Because deposition can produce corrosive HF gas, fluorinated precursors have been omitted from this study.

2. Experimental

2.1. Materials

Tungsten hexacarbonyl ($\text{W}(\text{CO})_6$), tetracarbonyl(1,5-cyclooctadiene)tungsten(0) ((1,5-cod) $\text{W}(\text{CO})_4$), bis(cyclopentadienyl)tungsten(IV) dihydride (WH_2Cp_2), and bis(isopropylcyclopentadienyl)tungsten(IV) dihydride ($\text{WH}_2(\text{iPrCp})_2$) were obtained from Sigma Aldrich; bis(*t*-butylimido)bis(dimethylamino)tungsten(VI) (BTBMW), and mesitylene tungsten tricarbonyl ((mes) $\text{W}(\text{CO})_3$) were obtained from Strem Chemicals; WCl_6 was obtained from Thermo Scientific Chemicals; WCl_5 was obtained from Entegris. Benzoic acid (Mettler-Toledo calibration substance, analytical standard) was obtained from Sigma-Aldrich, and salicylic acid (certified ACS grade) was obtained from Fisher Chemical.

(mes) $\text{W}(\text{CO})_3$ was purified by sublimation prior to use based on a published method.¹⁴ In short, a sublimation apparatus was filled, in a N_2 -atmosphere glovebox, with ~ 1 g (mes) $\text{W}(\text{CO})_3$ and connected to a Schlenk line. The cold finger was connected to a chiller set to 9.5 °C, and the bottom of the sublimation apparatus was submerged into an oil bath which was then heated to 145 °C. Meanwhile, the pressure in the sublimation apparatus was lowered to ~ 50 mTorr. After a few hours, the apparatus was taken back into the glovebox and the sublimed yellow product was collected ($\sim 45\%$ of the original loading). All other reagents were used as received without further purification.

2.2. Thermogravimetric analysis

All TGA experiments were conducted on an ISI TGA-1000 instrument inside of a N_2 -atmosphere glovebox, with a $5 \text{ cm}^3 \text{ min}^{-1}$ flow of ultra-high purity N_2 . A platinum pan (surface area $3.44 \times 10^{-5} \text{ m}^2$) was used as a sample holder in all trials.

Precursors were spread evenly across the entire surface of the pan. All measurements were conducted non-isothermally at a constant temperature ramp rate of $10\text{ }^{\circ}\text{C min}^{-1}$ and nominal sample loadings of 3, 5, 8, and 10 mg; as well as a constant nominal sample loading of 3 mg with temperature ramp rates of 5, 10, 15, and $20\text{ }^{\circ}\text{C min}^{-1}$. $\text{W}(\text{CO})_6$ and BTBMW were analyzed from $25\text{ }^{\circ}\text{C}$ up to $200\text{ }^{\circ}\text{C}$; $\text{WH}_2(\text{iPrCp})_2$ was analyzed from $25\text{--}300\text{ }^{\circ}\text{C}$; and $(1,5\text{-cod})\text{W}(\text{CO})_4$, $\text{WH}_2(\text{Cp})_2$, WCl_6 , $[\text{WCl}_5]_2$, and $(\text{mes})\text{W}(\text{CO})_3$ were analyzed from $25\text{--}400\text{ }^{\circ}\text{C}$.

Benzoic acid and salicylic acid standards were analyzed for calibration purposes from RT up to $200\text{ }^{\circ}\text{C}$, at sample masses of 2 mg, and these trials were repeated three times.

2.3. Atomic layer deposition

A Fiji Gen2 PEALD system from Veeco® with an Ebara® multistage dry vacuum pump A30W (pumping speed 3600 l min^{-1}) was used to attempt to deposit WO_3 films on glass slides and silicon wafers with $(\text{mes})\text{W}(\text{CO})_3$ as the W source. Substrates were ultrasonically cleaned with isopropyl alcohol and deionized water (DIW) and blown dry with nitrogen, which was followed by a 5 min exposure to UV- O_3 conducted on an Ossila® Model E511. The ultimate base pressure of the ALD chamber was maintained at 5.25×10^{-7} Torr with a working pressure of 215 mTorr. The ALD chamber, delivery line and ampoule temperatures are varied according to Table 1.

Previously, one of our groups reported an *in situ* spectroscopic ellipsometry approach for the rapid development of ALD processes. This innovative approach deviates from conventional ALD process optimization recipes in that the pulse time leading to dose saturation is established across a range of temperatures in a single set of experiments. Ten consecutive pulses of precursor are introduced into the chamber with each pulse separated by an argon (Ar) purge. This is then followed by ten consecutive pulses of the oxidant, again with each pulse separated by Ar purge. Thus, in a single sequence of 10 pulses of precursor and oxidant a complete ALD pulse sequence can be mapped. Conducting the same process at different temperatures produces a temperature–(pulse) time–thickness (TTT) graph.¹⁵

Sets of ALD experiments were conducted with $(\text{mes})\text{W}(\text{CO})_3$, with de-ionized water (DIW), remote O_2 plasma, or O_2 gas as the oxidant. For the present case, ten pulses of $(\text{mes})\text{W}(\text{CO})_3$ were dosed into the chamber with each pulse separated by a 10 s Ar purge followed by ten consecutive pulses of oxidant each separated by a 10 s Ar purge. Chamber conditions were tested first at $175\text{ }^{\circ}\text{C}$ with ampoule temperatures of 80, 100, and $120\text{ }^{\circ}\text{C}$ as detailed in Table 1 runs 1–7. In the second test the chamber was set to $225\text{ }^{\circ}\text{C}$ with ampoule temperatures of 120 and $140\text{ }^{\circ}\text{C}$, and growth was attempted with conventional alternating precursor-purge-oxidant-purge pulses (Table 1, runs 8–12). In each test $(\text{mes})\text{W}(\text{CO})_3$ did build up pressure in the ampoule commensurate with volatility but did not yield a reliable ALD growth.

The deposition rate of the film was monitored by *in situ* spectroscopic ellipsometry using a J. A. Woollam® M-2000, with a wavelength range from 273 to 1690 nm. The thickness was modeled using the CompleteEASE® software, consisting of a Cauchy layer optimized with tungsten oxide optical constants on a SiO_2 substrate layer.

3. Results and discussion

Precursor behavior was studied by non-isothermal TGA experiments, at a constant temperature ramp rate and with varying sample masses. Results were validated by measuring non-isothermal TGA experiments at fixed (*approximately*) precursor mass, with varying temperature ramp rates. TG curves are plotted as percent mass *versus* temperature. As a figure of comparison, the temperature range in which a precursor undergoes sublimation is designated the “TGA temperature window” of that precursor; specifically, the region between 5% and 95% of observed mass loss (Fig. 2A). Notably, *this is not to be confused with ALD temperature windows as reported in literature*, which are determined by ALD growth processes. The measured TGA temperature window is dependent on the sample mass and the temperature ramp rate. The sublimation kinetics are a function of the surface area of the precursor, which is equal to

Table 1 Experimental conditions for ALD trials using $(\text{mes})\text{W}(\text{CO})_3$

Run	Chamber temp. ($^{\circ}\text{C}$)	Line temp. ($^{\circ}\text{C}$)	Ampoule temp. ($^{\circ}\text{C}$)	Pulse time (s)	Oxidant (pulse time, s)
1	175	120	80	0.06	300 W O_2 plasma (4)
2	175	120	80	0.10	300 W O_2 plasma (4)
3	175	120	100	0.06	300 W O_2 plasma (4)
4	175	120	100	0.06	80 sccm O_2 (10)
5	175	120	100	0.06	H_2O (0.06)
6	175	150	120	0.06	H_2O (0.06)
7	175	150	120	0.12	H_2O (0.06)
^a 8	175	150	120	0.12	H_2O (0.06)
^a 9	175	150	120	0.5	50 W O_2 plasma (4)
^a 10	175	150	120	0.5	25 W O_2 plasma (4)
^a 11	225	150	120	0.5	25 W O_2 plasma (4)
^a 12	225	150	140	0.5	25 W O_2 plasma (4)

^a (8–12) note long form process over 50 cycles using standard alternating pulses of precursor, purge and oxidant, the remaining (1–7) were conducted for $\times 10$ TTT as described in the text.

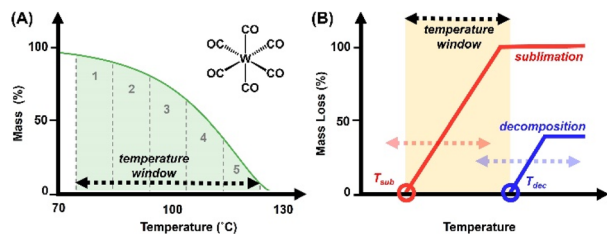


Fig. 2 (A) TGA trace of $W(CO)_6$ with highlighted "TGA temperature window" and illustration of sequestered zones utilized for calculation of E_a and ΔH_{sub} . (B) General schematic to illustrate the correlation of precursor volatility and stability juxtaposed against the potential ALD temperature window.

the surface area of the TGA pan; a platinum pan with a bottom measuring $3.44 \times 10^{-5} \text{ m}^2$. As the surface area remains constant, an increase in the ramp rate shifts the temperature window towards higher temperatures (which are attained more rapidly), while sublimation rates remain limited by the surface area of the TGA pan.

Ultimately, the TGA temperature window serves as a preliminary surrogate for the downstream ALD temperature window. Ideally, precursor volatilization (onset at the temperature of sublimation, T_{sub}) is complete prior to onset of decomposition (T_{dec}), *i.e.*, T_{dec} sits beyond the TGA temperature window (Fig. 2B). This scenario typically results in little or no residual mass on the TGA pan, and in terms of ALD applicability implies viable delivery of a precursor without thermally induced decomposition which would result in CVD-type growth. The closer the T_{dec} lies to the temperature window, the higher the associated residual mass as measured by TGA. The latter can be triggered by high temperature ramp rates and/or higher sample masses, where T_{dec} is reached prior to complete volatilization.

The obtained TGA traces were sectioned off to five equivalent zones within the established TGA temperature window (Fig. 2A), and the extracted values facilitated the calculation of activation energies (E_a) and enthalpies of sublimation (ΔH_{sub}) for all precursors (Scheme 1). Lower values of E_a and ΔH_{sub} are associated with more volatile precursors. A complete and detailed description of how these values are obtained has been provided in our prior publication.¹⁶ We note that the measurements performed on the W precursors were conducted in concert with our previously reported Mo precursor chemistry, thus the calibration data for the TGA instrument is identical; as measured with a benzoic acid standard and corroborated with a salicylic acid standard. Finally, a plot of the natural log of $1/\text{Torr}$ versus T ($^\circ\text{C}$) was created within the TGA temperature window, to which a linear trendline was fitted and used to calculate the temperature at 1 Torr. An example of these measurements for $W(CO)_6$ is highlighted in Fig. 3.

The average values for E_a and ΔH_{sub} determined for the *ca.* 3, 5, 8, and 10 mg precursor samples are shown in Table 2 (and mapped in Fig. 4) along with their respective derived temperatures at 1 Torr pressure, and the residual masses. In parallel, all molecules were studied by non-isothermal TGA experiments, at a constant mass of *ca.* 3 mg and variable temperature ramp rates of 5, 10, 15, and $20 \text{ }^\circ\text{C min}^{-1}$. The resulting values appear

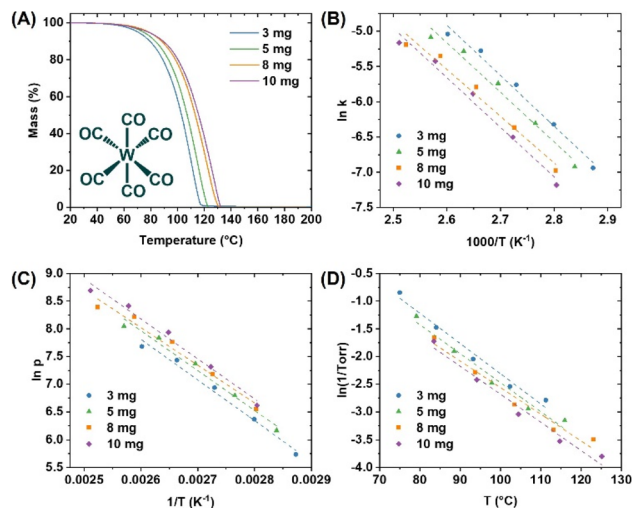


Fig. 3 Thermogravimetric analysis of $W(CO)_6$: (A) precursor TG trace at a constant temperature ramp rate of $10 \text{ }^\circ\text{C min}^{-1}$; (B) the Arrhenius plot (E_a is obtained from the slope of the curves via $-E_a/R$); (C) plot of $\ln p$ vs. $1/T$, the enthalpy of sublimation is derived from the slope of the straight lines, which is equal to $-\Delta H_{sub}/R$; (D) plot of $\ln(1/\text{Torr})$ vs. T , used to extrapolate the 1 Torr temperature. R = ideal gas constant $8.314 \text{ J K}^{-1} \text{ mol}^{-1}$ (p = kPa).

similar and are included in the ESI† as further validation of the consistency of the methodology used (Table S17†). Direct comparison of values to literature is difficult due to variability introduced by the measurement techniques; nonetheless, the ΔH_{sub} values obtained herein are reasonable and correlate to prior reports. For example $W(CO)_6$ ΔH_{sub} obtained herein is $59.4 \pm 1.9 \text{ kJ mol}^{-1}$ compared to a broad range from 69.9 ± 4.2 to $78.9 \pm 1.1 \text{ kJ mol}^{-1}$ from the prior literature.^{17–21} WH_2Cp_2 resides even closer to the prior literature with a ΔH_{sub} value of $85.3 \pm 7.8 \text{ kJ mol}^{-1}$, compared to $84.1 \pm 1.6 \text{ kJ mol}^{-1}$ reported by Dias and coworkers.²² Critically, while there may be discrepancies across experimental ΔH_{sub} across both the prior literature and the values reported herein, the experimental values across the molecules studied herein are self-consistent which facilitates a direct comparison. This would otherwise be difficult to achieve by collating previously published data across multiple sources.

Analysis of most precursors revealed very minimal residual mass. Notably, both (1,5-cod) $W(CO)_4$ and (mes) $W(CO)_3$ yielded non-trivial amounts of residual mass (19.5 ± 0.4 and $48.9 \pm 0.8\%$, respectively). This is indicative of competing decomposition in addition to sublimation. For (1,5-cod) $W(CO)_4$ the residual mass was nonetheless significantly lower than the W metal content of 45.5%, implying a reasonable amount of sublimation prior to decomposition of the ligand framework. This is evident in the well-behaved TGA trace which could be treated similarly as the remaining precursors to extract relevant E_a , ΔH_{sub} , and 1 Torr temperature values (Fig. S9†). Conversely, the residual mass from (mes) $W(CO)_3$ was significantly high at 48.9%, implying a significant amount of decomposition (Fig. 5A). It should be noted that (mes) $W(CO)_3$ was purified by sublimation under vacuum,¹⁴ thus it is well established that it

Table 2 TGA-derived E_a , ΔH_{sub} and 1 Torr temperature values from trials varying mass, with fixed $10\text{ }^\circ\text{C min}^{-1}$ heating rate^a

Molecule	E_a (J mol^{-1})	ΔH_{sub} (kJ mol^{-1})	T at 1 Torr ($^\circ\text{C}$)	Res. mass (%)
$\text{W}(\text{CO})_6$	57.8 ± 1.9	59.4 ± 1.9	51.0 ± 5.3	0.0 ± 0.0
$(1,5\text{-cod})\text{W}(\text{CO})_4$	148.5 ± 17.7	150.7 ± 17.3	150.5 ± 1.4	19.5 ± 0.4
WH_2Cp_2	83.3 ± 7.8	85.3 ± 7.8	136.4 ± 8.5	0.6 ± 0.0
$\text{WH}_2(\text{iPrCp})_2$	47.7 ± 8.0	49.6 ± 8.0	109.8 ± 6.4	0.3 ± 0.3
BTBMW	47.4 ± 4.7	49.0 ± 4.8	61.6 ± 1.8	1.5 ± 0.5
WCl_6	79.5 ± 14.0	81.3 ± 14.0	142.1 ± 8.3	1.2 ± 2.5
$[\text{WCl}_5]_2$	66.5 ± 14.2	68.3 ± 14.2	117.9 ± 14.9	1.0 ± 0.3

^a Note $(\text{mes})\text{W}(\text{CO})_3$ led predominantly to decomposition products with $48.9 \pm 0.8\%$ residual mass precluding extraction of sublimation kinetics.

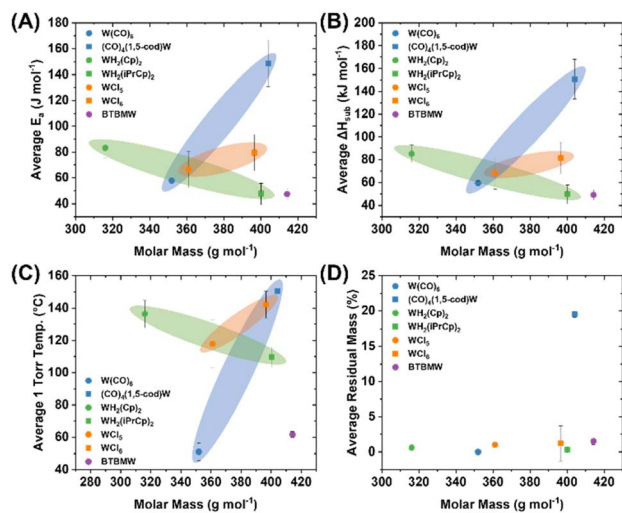


Fig. 4 TGA-derived average (A) E_a , (B) ΔH_{sub} , (C) 1 Torr temperature, and (D) residual mass values from trials varying mass, with fixed $10\text{ }^\circ\text{C min}^{-1}$ heating rate, plotted against the molar mass of the precursor molecules.

can indeed be volatilized; however, it is clear that the decomposition range overlaps significantly with the TGA temperature window (Fig. 5B). For this reason, reliable E_a , ΔH_{sub} , and 1 Torr temperature values could not be extracted and were omitted from Table 2 and Fig. 4.

Averaged E_a , ΔH_{sub} , 1 Torr temperature, and residual mass percentage values were mapped visually as a function of their molar masses (Fig. 4), with precursor molecules categorized according to their general ligand classes; carbonyls [$\text{W}(\text{CO})_6$, $(1,5\text{-cod})\text{W}(\text{CO})_4$], cyclopentadienyl [WH_2Cp_2 , $\text{WH}_2(\text{iPrCp})_2$], chlorides [$[\text{WCl}_5]_2$, WCl_6], and amino/imido [BTBMW].

While no clear linear trend emerges among the whole group, there are clear trends within the related molecule groups. Both the carbonyls [$\text{W}(\text{CO})_6$, $(1,5\text{-cod})\text{W}(\text{CO})_4$] and chlorides [$[\text{WCl}_5]_2$, WCl_6] show an increase in E_a , ΔH_{sub} and 1 Torr temperature commensurate with increasing molar mass. Note, while WCl_5 is depicted as a dimer [$[\text{WCl}_5]_2$], that is indicative of the solid state structure, it dissociates to WCl_5 monomer upon evaporation.²³ Conversely, among the cyclopentadienyls, $\text{WH}_2(\text{iPrCp})_2$ displays significantly lower E_a , ΔH_{sub} and 1 Torr temperatures than WH_2Cp_2 despite a molar mass difference of $+84.16\text{ g mol}^{-1}$. Namely, the E_a is 43% lower, the ΔH_{sub} is 42% lower, while the molar mass is 27% higher for $\text{WH}_2(\text{iPrCp})_2$. The presence of the *iPr* group comparatively lowers the symmetry of the molecule rendering it liquid at room temperature, compared to WH_2Cp_2 which is a crystalline solid at room temperature, with a reported melting point at $\sim 115\text{ }^\circ\text{C}$.²⁴ BTBMW, another liquid at room temperature (likely aided by the presence of the *tBu* groups), displayed the lowest E_a , ΔH_{sub} and 1 Torr temperatures despite having the highest molar mass of all molecules tested (414.23 g mol^{-1}). It is noteworthy how much of an impact the introduction of bulky functional groups that can inhibit crystalline packing, and in this case render the material liquid, has on achieving rapid volatility, as compared to simply lowering the molecular mass. The latter is typically done by choosing smaller ligands, which are often more symmetrical and result in crystalline solids at room temperature.

Among the non-halides, and to the best of our knowledge, $\text{W}(\text{CO})_6$,^{25–28} WH_2Cp_2 ,^{25,29} $\text{WH}_2(\text{iPrCp})_2$,^{30,31} and BTBMW^{25,32–39} have been successfully utilized for ALD processes, whereas all have been utilized for CVD^{39–48} (halides included^{48–54}). While $(1,5\text{-cod})\text{W}(\text{CO})_4$ exhibits higher-than-average E_a , ΔH_{sub} and residual mass values, the temperature window falls within currently useable range, and is likely adaptable to an ALD growth process. The higher-than-average E_a and ΔH_{sub} values can be readily mitigated through the use of low vapor pressure ALD precursor delivery systems. On the contrary, and as noted above, the residual mass from $(\text{mes})\text{W}(\text{CO})_3$ was significantly high which implied a significant amount of decomposition within the sublimation temperature window (Fig. 5A). Based on the implication of TGA screening as a prognosticator for ALD precursor viability, this result implies that $(\text{mes})\text{W}(\text{CO})_3$ would not be a feasible precursor. However, as the molecule was readily sublimed under vacuum (using standard Schlenk line

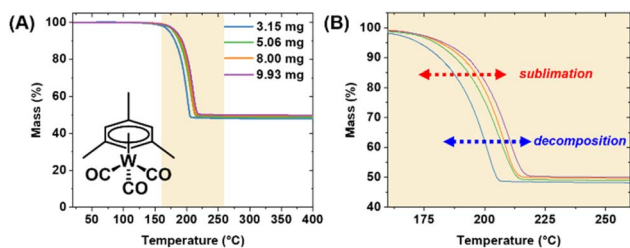


Fig. 5 (A) TGA traces of $(\text{mes})\text{W}(\text{CO})_3$ at varying masses with a temperature ramp rate of $10\text{ }^\circ\text{C min}^{-1}$. (B) Close up region where volatility is observed, highlighting overlapping sublimation and decomposition events.

techniques with a standard vacuum set up at ~ 50 mTorr) for purification, it warranted further testing for validation.

To test viability for ALD growth of WO_x , experiments were conducted with (mes)W(CO)₃, and DIW, remote O₂ plasma, and O₂ gas as the oxidant. Further details are found in the experimental section. Chamber temperatures were tested initially at 175 °C with ampoule/precursor temperatures of 80, 100, and 120 °C. Subsequently the chamber was set to 225 °C and the ampoule temperatures at 120 and 140 °C. In each test there was a noted buildup of pressure in the ampoule commensurate with generation of volatile compounds, but ultimately reliable ALD growth could not be achieved under any of the conditions noted. Based on the ALD results, and the TGA trials, it appears that precursor decomposition is the dominant route within the observed window of volatility (Fig. 5B), and very likely, the majority of pressure build up within the ampoule was the generation of volatile organics and CO. Thus while (mes)W(CO)₃ can be purified at elevated temperature by sublimation under continuous vacuum, TGA analysis under N₂ flow (instead of reduced pressure), and incubation within an ALD ampoule commensurate with pulsed delivery leads in both latter cases predominantly to decomposition products. Thus, the TGA analysis herein is adequately predictive for the non-feasibility of (mes)W(CO)₃ for standard ALD but does not preclude potential applications in various CVD processes where the precursor can be delivered continuously or using a stabilizing solvent carrier.

4. Conclusions

The volatility and thermal stability of eight commercially available CVD and ALD molecular precursors based on W were evaluated by non-isothermal TGA experiments. Precursor ceramic yields and ALD temperature windows were obtained directly from the TGA plots. Activation energy (E_a), enthalpy of sublimation (ΔH_{sub}), and 1 Torr temperature values were determined from the TGA data. Because these values are dependent on experimental set-up, a direct comparison of such values collected across variable literature reports is complicated. Our report provides a unified, and rigorous comparison of such values, which can serve as a quick reference map of temperature windows to rapidly match to desired temperature regimes for W-based film growth. A closer look at volatility trends among the various molecule ligand groupings, and at large, reveals the importance of ligand design choice, namely introduction of bulky, symmetry-lowering substituents to prevent crystallinity and afford low ΔH_{sub} values. Moreover, the predicting factor of TGA screening was juxtaposed with known material volatility when the TGA trials for (mes)W(CO)₃ pointed to low feasibility for ALD application. Therein, attempted ALD growth of WO_x under a variety of conditions yielded no thin films, validating the TGA screening approach.

Data availability

All measured TGA experiments are provided as plots in the ESI.† Data generated by TGA measurements⁵⁵ is available from the Materials Data Facility.^{56,57}

Conflicts of interest

There are no conflicts to declare.

Acknowledgements

This work was supported by the Department of Chemistry (College of Sciences), the Department of Materials Science and Engineering (College of Engineering and Computer Science) and the Faculty Cluster Initiative at the University of Central Florida. The authors thank NSF Award 2121953 and the PREM Center for Ultrafast Dynamics and Catalysis in Emerging Materials for partially supporting this work. SNB was supported by the GEM fellowship and SRC award number 3026.001. PB and TM-J were supported by NSF award number 2424976.

References

- 1 J. Lu, B. Fu, M. C. Kung, G. Xiao, J. W. Elam, H. H. Kung and P. C. Stair, *Science*, 2012, **335**, 1205–1208.
- 2 H. Yan, H. Cheng, H. Yi, Y. Lin, T. Yao, C. Wang, J. Li, S. Wei and J. Lu, *J. Am. Chem. Soc.*, 2015, **137**, 10484–10487.
- 3 K. Galatsis, Y. Li, W. Wlodarski and K. Kalantar-Zadeh, *Sens. Actuators, B*, 2001, **77**, 478–483.
- 4 M. Ferroni, V. Guidi, G. Martinelli, P. Nelli, M. Sacerdoti and G. Sberveglieri, *Thin Solid Films*, 1997, **307**, 148–151.
- 5 M. Chhowalla and G. A. Amaratunga, *Nature*, 2000, **407**, 164–167.
- 6 M. Bivour, J. Temmler, H. Steinkemper and M. Hermle, *Sol. Energy Mater. Sol. Cells*, 2015, **142**, 34–41.
- 7 J. Lu, J. W. Elam and P. C. Stair, *Surf. Sci. Rep.*, 2016, **71**, 410–472.
- 8 R. W. Johnson, A. Hultqvist and S. F. Bent, *Mater. Today*, 2014, **17**, 236–246.
- 9 A. S. Asundi, J. A. Raiford and S. F. Bent, *ACS Energy Lett.*, 2019, **4**, 908–925.
- 10 S. T. Barry, *Coord. Chem. Rev.*, 2013, **257**, 3192–3201.
- 11 F. Zaera, *Coord. Chem. Rev.*, 2013, **257**, 3177–3191.
- 12 L. K. Tan, B. Liu, J. H. Teng, S. Guo, H. Y. Low and K. P. Loh, *Nanoscale*, 2014, **6**, 10584–10588.
- 13 D. Seghete, G. Rayner Jr, A. Cavanagh, V. Anderson and S. George, *Chem. Mater.*, 2011, **23**, 1668–1678.
- 14 R. B. King and A. Fronzaglia, *Inorg. Chem.*, 1966, **5**, 1837–1846.
- 15 U. Kumar, C. Feit, S. N. Berriel, A. Arunachalam, T. S. Sakthivel, K. Basu, P. Banerjee and S. Seal, *J. Vac. Sci. Technol., A*, 2021, **39**, 060405.
- 16 T. E. Shaw, Z. Ali, T. M. Currie, S. N. Berriel, B. Butkus, J. T. Wagner, K. Preradovic, G. P. A. Yap, J. C. Green, P. Banerjee, A. P. Sattelberger, L. McElwee-White and T. Jurca, *ACS Appl. Mater. Interfaces*, 2023, **15**, 35590–35599.
- 17 M. L. Garner, D. Chandra and K. H. Lau, *J. Phase Equilib.*, 1995, **16**, 24–29.
- 18 A. Baev, *Zh. Fiz. Khim.*, 1993, **67**, 2399–2402.
- 19 R. M. Stephenson, *Handbook of the Thermodynamics of Organic Compounds*, Springer Science & Business Media, 2012.

- 20 G. Boxhoorn, J. M. Ernstring, D. J. Stufkens and A. Oskam, *Thermochim. Acta*, 1980, **42**, 315–321.
- 21 H. Daamen, J. M. Ernstring and A. Oskam, *Thermochim. Acta*, 1979, **33**, 217–223.
- 22 A. Dias, H. Diogo, M. Minas da Piedade and J. Simoes, *J. Organomet. Chem.*, 1990, **391**, 361.
- 23 F. A. Cotton and C. E. Rice, *Acta Crystallogr. B*, 1978, **34**, 2833–2834.
- 24 Sigma-Aldrich, *Bis(cyclopentadienyl)tungsten(IV) dihydride Safety Data Sheet*, <https://www.sigmaaldrich.cn/CN/en/sds/aldrich/510807>, accessed September 13, 2024.
- 25 H. Shimizu, K. Shima, Y. Suzuki, T. Momose and Y. Shimogaki, *J. Mater. Chem. C*, 2015, **3**, 2500–2510.
- 26 D. K. Nandi, U. K. Sen, S. Sinha, A. Dhara, S. Mitra and S. K. Sarkar, *Phys. Chem. Chem. Phys.*, 2015, **17**, 17445–17453.
- 27 J. Malm, T. Sajavaara and M. Karppinen, *J. Chem. Vap. Deposition*, 2012, **18**, 245–248.
- 28 D. K. Nandi, U. K. Sen, A. Dhara, S. Mitra and S. K. Sarkar, *RSC Adv.*, 2016, **6**, 38024–38032.
- 29 H. Shimizu, K. Sakoda, T. Momose and Y. Shimogaki, *Jpn. J. Appl. Phys.*, 2012, **51**, 05EB02.
- 30 K. Y. Ko, J.-G. Song, Y. Kim, T. Choi, S. Shin, C. W. Lee, K. Lee, J. Koo, H. Lee and J. Kim, *ACS Nano*, 2016, **10**, 9287–9296.
- 31 J.-G. Song, J. Park, W. Lee, T. Choi, H. Jung, C. W. Lee, S.-H. Hwang, J. M. Myoung, J.-H. Jung and S.-H. Kim, *ACS Nano*, 2013, **7**, 11333–11340.
- 32 J. S. Becker and R. G. Gordon, *Appl. Phys. Lett.*, 2003, **82**, 2239–2241.
- 33 J. S. Becker, S. Suh, S. Wang and R. G. Gordon, *Chem. Mater.*, 2003, **15**, 2969–2976.
- 34 O. Zandi, J. A. Beardslee and T. Hamann, *J. Phys. Chem. C*, 2014, **118**, 16494–16503.
- 35 D.-H. Kim, Y. J. Kim, Y. S. Song, B.-T. Lee, J. H. Kim, S. Suh and R. Gordon, *J. Electrochem. Soc.*, 2003, **150**, C740.
- 36 S. Balasubramanyam, M. J. Merckx, M. A. Verheijen, W. M. Kessels, A. J. Mackus and A. A. Bol, *ACS Mater. Lett.*, 2020, **2**, 511–518.
- 37 Y. Wu, M. H. Raza, Y.-C. Chen, P. Amsalem, S. Wahl, K. Skrodczky, X. Xu, K. S. Lokare, M. Zhukush and P. Gaval, *Chem. Mater.*, 2019, **31**, 1881–1890.
- 38 M. J. Sowa, Y. Yemane, F. B. Prinz and J. Provine, *J. Vac. Sci. Technol., A*, 2016, **34**, 051516.
- 39 H. Shimizu, Y. Suzuki, T. Nogami, N. Tajima, T. Momose, Y. Kobayashi and Y. Shimogaki, *ECS J. Solid State Sci. Technol.*, 2013, **2**, P311.
- 40 K. K. Lai and H. H. Lamb, *Chem. Mater.*, 1995, **7**, 2284–2292.
- 41 S. M. Eichfeld, L. Hossain, Y.-C. Lin, A. F. Piasecki, B. Kupp, A. G. Birdwell, R. A. Burke, N. Lu, X. Peng and J. Li, *ACS Nano*, 2015, **9**, 2080–2087.
- 42 M. Ishida, J. Fujita, T. Ichihashi, Y. Ochiai, T. Kaito and S. Matsui, *J. Vac. Sci. Technol., B: Microelectron. Nanometer Struct.–Process., Meas., Phenom.*, 2003, **21**, 2728–2731.
- 43 Y.-M. Sun, S. Lee, A. Lemonds, E. Engbrecht, S. Veldman, J. Lozano, J. White, J. Ekerdt, I. Emesh and K. Pfeifer, *Thin Solid Films*, 2001, **397**, 109–115.
- 44 H. Shimizu, K. Sakoda and Y. Shimogaki, *Microelectron. Eng.*, 2013, **106**, 91–95.
- 45 C. Spee, F. Verbeek, J. Kraaijkamp, J. Linden, T. Rutten, H. Delhay, E. Van der Zouwen and H. Meinema, *Mater. Sci. Eng. B*, 1993, **17**, 108–111.
- 46 A. Ogura, S. Imai, T. Kagawa, H. Kurozaki, M. Ishikawa, I. Muramoto, H. Machida and Y. Ohshita, *J. Vac. Sci. Technol., A*, 2008, **26**, 561–564.
- 47 T. W.-K. Yeow, K. Mistry, A. Shahin, M. Yavuz and K. P. Musselman, *J. Vac. Sci. Technol., A*, 2020, **38**, 052411.
- 48 Y. Pauleau, *Thin Solid Films*, 1984, **122**, 243–258.
- 49 H. Bamnolker, R. Humayun, J. Gao, M. Danek and J. Collins, *US Pat.*, 9595470B2, 2017.
- 50 S. Ashraf, C. S. Blackman, S. C. Naisbitt and I. P. Parkin, *Meas. Sci. Technol.*, 2008, **19**, 025203.
- 51 C. S. Blackman and I. P. Parkin, *Chem. Mater.*, 2005, **17**, 1583–1590.
- 52 M. Nagai, N. Hirano and S. Omi, *Jpn. J. Appl. Phys.*, 2000, **39**, 4558.
- 53 F. Trincat, J. Regolini, J. Mercier and D. Bensahel, *Appl. Phys. Lett.*, 1991, **59**, 3291–3293.
- 54 X. Tang, R. Haubner, B. Lux and B. Kieffer, *J. Phys. IV*, 1995, **5**, 1013–1020.
- 55 T. M. Currie, T. McNealy-James, S. N. Berriel, K. Preradovic, A. P. Sattelberger, P. Banerjee and T. Jurca, *Materials Data Facility*, 2024, DOI: [10.18126/ga5y-dh42](https://doi.org/10.18126/ga5y-dh42).
- 56 B. Blaiszik, K. Chard, J. Pruyne, R. Ananthakrishnan, S. Tuecke and I. Foster, *JOM*, 2016, **68**, 2045–2052.
- 57 B. Blaiszik, L. Ward, M. Schwarting, J. Gaff, R. Chard, D. Pike, K. Chard and I. Foster, *MRS Commun.*, 2019, **9**, 1125–1133.